Viscoelastic creep of vertically aligned carbon nanotubes

2010 J. Phys. D: Appl. Phys. 43 315401

(http://iopscience.iop.org/0022-3727/43/31/315401)

J. Phys. D: Appl. Phys. **43** (2010) 315401 (7pp) doi:10.1088/0022-3727/43/31/315401

Viscoelastic creep of vertically aligned carbon nanotubes

Q Zhang[1], Y C Lu[2,5], F Du[1], L Dai[1,3], J Baur[4] and D C Foster[4]

[1] University of Dayton, 300 College Park, Dayton, OH 45469-0060, USA
[2] University of Kentucky, Lexington, KY 40506, USA
[3] Case Western Reserve University, 10900 Euclid Avenue, Cleveland, OH 44106-7217, USA
[4] Air Force Research Laboratory, Materials and Manufacturing Directorate, AFRL/RXBC, Wright-Patterson AFB, OH 45433, USA

Received 29 April 2010, in final form 28 June 2010
Published 16 July 2010
Online at stacks.iop.org/JPhysD/43/315401

Abstract
The paper reports the viscous creep occurring in vertically aligned carbon nanotubes (VA-CNTs). Nanoindentation experiments are conducted to characterize the creep behaviour of the nanotube materials. By recording the instantaneous control stress and strain rate, the creep strain rate sensitivity of the VA-CNT array is calculated. The creep property is found to depend upon the density of nanotube arrays.

(Some figures in this article are in colour only in the electronic version)

1. Introduction

Vertically aligned carbon nanotubes (VA-CNTs) have drawn considerable interest recently due to their new physical phenomena attractive for a large range of potential applications. The VA-CNT arrays or films have been investigated as field emission electron sources [1], electrical interconnects [2] and thermal interface materials [3]. The materials are likely structures for use in microelectronic devices and microelectromechanical systems [4]. In addition to the conventional VA-CNTs grown on planar substrates, large-scale CNTs have recently been grown on microscale carbon fibres [5, 6]. The VA-CNTs coated on carbon fibres can be potentially used as stress and strain sensors for modifying the fibre–matrix interfaces in composite materials [7], and as artificial hair flow sensors for use on micro-air vehicles.

In all these applications, the mechanical properties of the carbon nanotube arrays play important roles in their ultimate success. Although the mechanical properties of the VA-CNTs have been explored (mostly through nanoindentation or similar techniques), most previous studies have been limited to the static, elastic type deformation. Recently, time (rate)-dependent viscoelastic deformation has been reported to occur in nanotube materials. Mesarovic *et al* [8] and McCarter *et al* [4] have reported the stress relaxation behaviour of carbon nanotube turfs under a spherical indenter. The time-dependent deformation is attributed to the contact movements occurred in neighbouring nanotubes. The standard linear solid (3-elements) model has been used to interpret the relaxation behaviour. Pathak *et al* [9] have shown that the nanotube forests exhibit frequency-dependent viscoelastic deformation. The phase angle tan δ measured from dynamic indentation on prior-bucking nanotube specimen can be as high as 0.1, an order of magnitude higher than that of typical polymer materials. Misra *et al* [10] have reported that the indentation load–depth responses of the nanotube forests are rate-dependent: the higher the indentation velocities, the stiffer the load–depth curves. Such behaviour has been attributed to 'the local densification' effects directly below the compressed area.

This paper reports the time-dependent creep deformation of the VA-CNT arrays. The creep tests were performed with a nanoindenter equipped with a spherical tip, from which the creep strain rate sensitivity, or creep constant, was obtained. The nanoindentation strain rate sensitivity experiment was probably first performed by Pollock *et al* [11] and has been subsequently used to examine the creep deformation of materials at small dimensions [12–16]. The strain rate sensitivity experiment typically involves loading the indenter at a high loading rate and then holding the load applied on the indenter constant while monitoring the displacement of the indenter as a function of time. Based upon the load and displacement histories, the instantaneous hardness and indentation strain rate can be calculated. The hardness–indentation strain rate pairs are then plotted on a log–log graph to determine the strain rate sensitivity.

[5] Author to whom any correspondence should be addresed.

2. Experimental procedures

2.1. Material preparation

The VA-CNTs were synthesized by low pressure chemical vapour deposition (CVD) of acetylene on $15 \times 15\,\text{mm}^2$ SiO_2/Si wafers. In a typical experiment, a 10 nm thick aluminium layer was coated on the wafers before the deposition of 3 nm Fe film in order to enhance the attachment of grown nanotubes on the silicon (Si) substrate. The VA-CNT arrays can adhere to the growth substrate under a more than $150\,\text{N}\,\text{cm}^{-2}$ pull force. The catalyst coated substrate was first inserted into the quartz tube furnace and remained at 450 °C in air for 10 min, followed by pumping the furnace chamber to a pressure less than 10 mTorr. Thereafter, the growth of the CNT arrays was achieved by flowing a mixture of gases of 48% Ar, 28% H_2, 24% C_2H_2 at 750 °C under 10–100 Torr for 10–20 min. The length of the resultant aligned VA-CNTs could be adjusted by controlling the deposition time and pressure. The nanotubes produced by the present procedure were multiwalled, 3–6 walls, and had a narrow uniform diameter distribution between 10 and 15 nm.

The microstructure and morphologies of the carbon nanotube samples were studied using scanning electron microscopy (SEM), a field emission Hatachi S800 SEM unit.

2.1.1. Viscoelastic nanoindentation testing. The viscoelastic creep tests were performed on a Nano Indenter XP (MTS Nano Instruments, Oak Ridge, TN) with a spherical indenter of tip radius of 150 μm. The resolutions for load and displacement are 50 nN and 0.01 nm, respectively. The as-grown nanotube arrays (nanotubes grown on silicon substrate) were tested. The as-grown VA-CNT arrays had the nominal dimensions of 10 mm (length) × 10 mm (width) × 500 μm (thickness). For the indentation tests, the indenter was brought into contact with the nanotube sample surface with the aid of an optical microscope. Standard indentation loading experiments were first performed to obtain the load–depth response of the VA-CNT arrays to be tested. In general, the load–depth response was linear elastic at small depths and then buckled at large depths. The typical buckling load was found to be approximately 4 mN or higher for these VA-CNT arrays. For the creep experiments, smaller loads (typically 1.4 mN) were used. To perform the indentation creep tests, the indenter was quickly ramped to a control load within 1 s (figure 1). When performing creep experiments with an indenter, it is often advantageous to use a fast loading rate of the indenter to ensure a much greater amount of creep during the constant-load hold. That way, the time required for a material to reach the steady-state stage can be minimized and the creep test can be completed in a timely manner. Experiments with different loading times were also conducted to evaluate the effect of ramping rate on the creep response. The indenter was then held at the constant load for a period of 600 s. The hold segment was followed by an unloading segment. During all experiments, the indenter loads and displacements were recorded as a function of time. The thermal drift rate during the experiments was controlled to be less than $0.1\,\text{nm}\,\text{s}^{-1}$. All

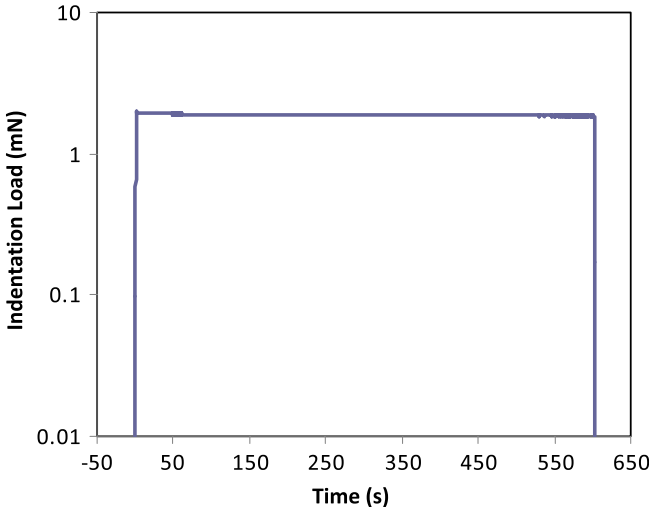

Figure 1. The load–time curve used in the nanoindentation creep experiments.

creep experiments reported here were conducted at ambient condition ($T = 23 \pm 0.5$ °C). The temperature was monitored by a LabView data acquisition system through several J-type thermocouples embedded inside the testing chamber.

3. Results and discussion

3.1. Morphology of the VA-CNT arrays

The surface morphology of the present nanotube specimens was examined by the SEM. Figures 2 and 3 show the side and top views of the specimen under various magnifications. As can be seen, the nanotubes are well-aligned perpendicularly to the substrate. The high magnification SEM images (figures 2(*b*) and (*c*)) show that the constituent individual nanotubes are somewhat zigzag-like along the nanotube length with some entanglements between the nanotubes as a result of the growth process. The areal density measurements for the VA-CNT samples were conducted by counting the number of nanotubes in the SEM image and then dividing the total number of nanotubes by the total area of the image. The average areal density of the current VA-CNT sample is $d_0 = 80\,\mu\text{m}^{-2}$.

Overall, the specimen has quite a smooth top surface that is suitable for the nanoindentation tests (figure 3(*a*)). A typical set of indentation tests (static and creep tests) would include indentation at multiple locations within a given array and the results have been found to be repeatable. Figure 3(*b*) shows the typical residual indentation mark obtained from a loading–unloading test. It should be noted that the load corresponding to this indentation is higher compared with the load used in typical creep experiments. The indentation obtained at higher load provides a better image of the deformation occurring during the indentation of VA-CNTs. It is seen that no material pile-up is observed around the indenter, indicating that the present nanotube array exhibits negligible strain hardening. Such observation is useful and implies that the contact depth between the indenter and the VA-CNTs can be estimated through the conventional formula (to be discussed in next section). If a material exhibits plastic pile-up

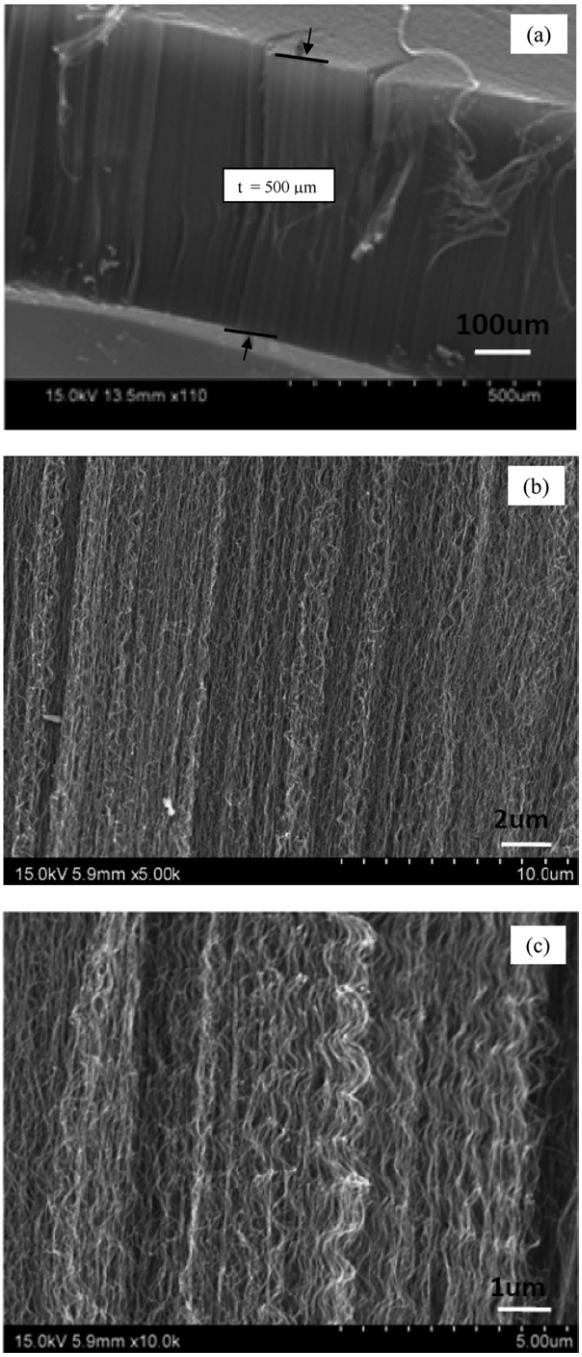

Figure 2. SEM micrographs showing the morphology of the side surface of the VA-CNT array ($t = 500\,\mu$m). (*a*)–(*c*) are SEM images with increasing magnification.

during indentation, the estimate for correct contact depth could become very complicated [17].

3.2. Load–depth response

A typical load–depth response of the VA-CNTs is shown in figure 4. The maximum load applied to the indenter was 2.5 mN and the indenter holding time was 5 s. The nanotube arrays used in the present experiments were grown on a rigid Si substrate. For a sample supported by a hard substrate, it is generally accepted that the indentation depth should not exceed 10% of the sample thickness ($h/t < 0.1$) in order to obtain the true load–depth response of the testing material [18]. The maximum indentation depth in the present experiments is seen to be approximately 4 μm (figure 4), an equivalent of indentation depth/sample thickness ratio $h/t \approx 0.01$. Within this small range of indentation, the influence of the Si substrate on the indentation response of the nanotube sample becomes negligible. The load–depth curve indicates that the VA-CNT array exhibits a typical elastic–plastic response. After withdrawing the indenter, the indented surface did not return to the original position, a sign of permanent deformation occurred in the sample. On the other hand, it is noticed that while held at a constant load, the indenter continues to penetrate into the specimen, indicating that the VA-CNT array exhibits creep deformation (insert in figure 4).

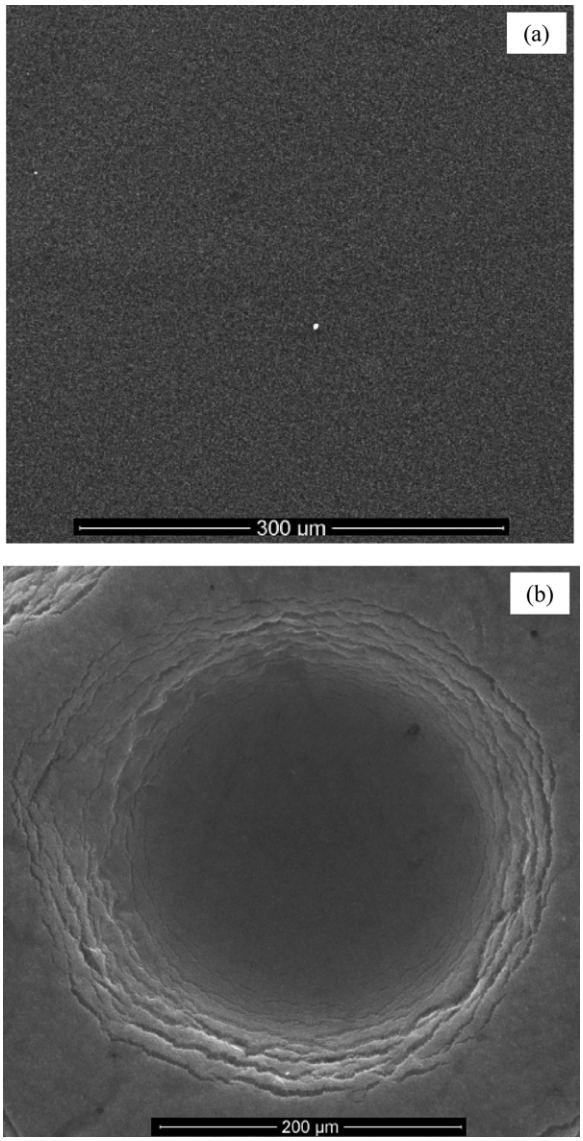

Figure 3. (*a*) SEM micrograph showing the morphology of the top surface of the VA-CNT array ($t = 500\,\mu$m). (*b*) SEM micrograph showing a residual indentation under spherical indenter of radius $R = 150\,\mu$m.

When indenting a viscoelatsic material, the creep displacement needs to be subtracted from the elastic contact depth formula. In addition, the contact depth between the

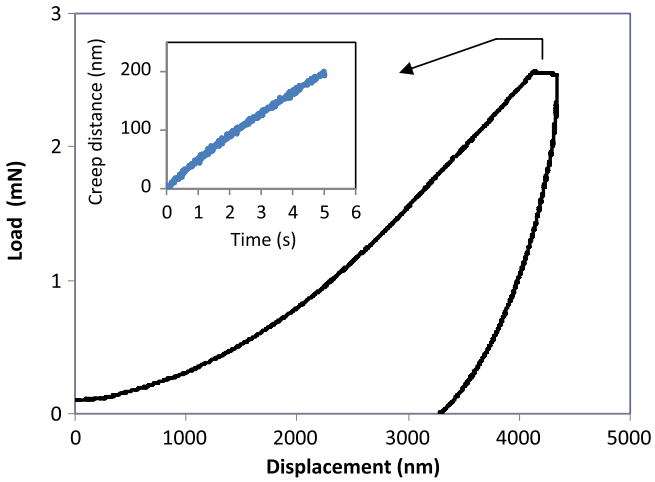

Figure 4. The typical load–depth curve of the VA-CNT array with a spherical indenter of $R = 150\,\mu$m. The indenter holding time is 5 s.

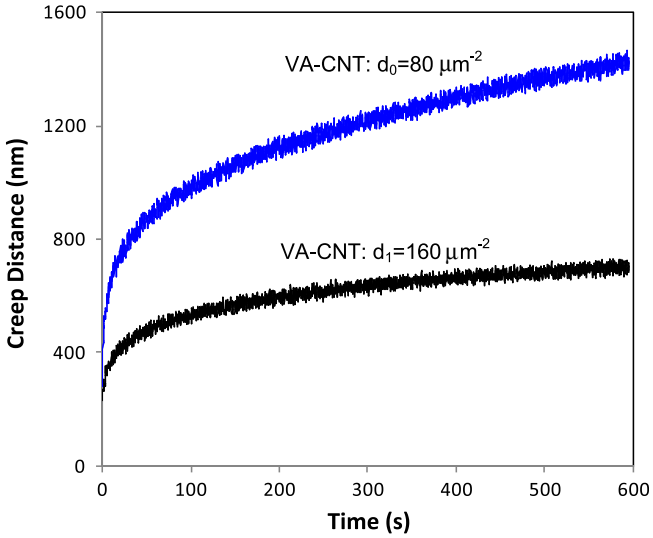

Figure 5. The indentation displacement–time curves of the VA-CNT arrays. The specimen with higher density was prepared by squeezing the original nanotube specimen by a volumetric factor of 2.

indenter and the specimen depends upon the indenter holding time and unloading rate. After taking these factors into account, the elastic contact depth (h_c) during the indentation of a viscoelastic material is determined as follows [19]:

$$h_c = (h_{max} - h_{creep}) - 0.75 P_{max}\left(\frac{1}{S} - \frac{\dot{h}_v}{\dot{P}}\right), \qquad (1)$$

where h_{max} is the maximum indentation depth, h_{creep} the change in the indentation depth during the holding time and P_{max} the peak load. S is the elastic stiffness as determined from the slope of the unload curve evaluated at the maximum depth ($S = (dP/dh)_{h=h_{max}}$). $\dot{h}_v$ is the creep rate at the end of the load hold and $\dot{P}$ the indenter unloading rate.

Once the contact depth is determined, the indenter–specimen contact radius a can be computed:

$$a = \sqrt{2h_c R - h_c^2}, \qquad (2)$$

where R is the indenter radius and h_c the actual contact depth of indenter and specimen.

After estimating the indenter–sample contact radius (a), the instantaneous modulus (E) can be calculated following the standard procedures [20]:

$$E = \frac{1 - \nu^2}{(1/E_r) - ((1 - \nu_i^2)/E_i)}, \qquad (3)$$

where $E_r = S/2 \cdot (1.034) \cdot a$ and E_i and ν_i are the elastic modulus and Poisson's ratio of the indenter (for diamond indenter: $E_i = 1140$ GPa and $\nu_i = 0.07$ [21]).

From the load–depth curve (figure 4), the contact stiffness of the VA-CNTs was determined as 0.003 87mN nm^{-1}. Using equation (3), the instantaneous modulus was determined as 58 MPa (by using a Poisson's ratio $\nu = 0$ [22]). This result seems to be consistent with the corresponding values reported in the literature [23–25]. Although the axial modulus of a single carbon nanotube (multiwalled) could be up to 1 TPa or higher [26–28], the moduli of the carbon nanotube arrays have been found to be much lower. That is because the intertube van der Waals interactions in the carbon nanotube arrays are weak and the individual tubes in the arrays can easily rotate and slide with respect to one another [25]. The actual modulus of the CNT arrays depends upon many factors, including the density and morphology of the specimens.

3.3. Viscoelastic creep

As evident in the load–depth curve (figure 4), the present VA-CNT arrays exhibit time-dependent deformation (i.e. creep). To conduct the creep experiments, a much longer holding time ($t = 600$ s) has been applied to the indenter tip. Figure 5 shows the indentation creep responses of VA-CNT arrays with different tube densities: $d_0 = 80\,\mu$m^{-2} and $d_1 = 160\,\mu$m^{-2}. The high density specimen was prepared by squeezing the original nanotube specimen by a volumetric factor of 2, according to a reported method [24]. The nanotube array with a higher density is seen to exhibit a lesser degree of creep. The result is in agreement with the numerical finding reported by Liew *et al* [25], who studied the effect of tube interspatial gap in CNT arrays using the molecular dynamics (MD) simulation. The CNT array with smaller interspatial gaps, or a higher tube density, tends to have higher buckling load. This is due to the possibility of the formation of covalent bonds among the individual tubes when the CNT specimen is squeezed.

The creep deformation of the nanotube materials can be divided into two stages: (1) transient and (2) steady state. In the steady state, the elastic deformation has no effect on the creep behaviour, and the indentation depth is a linear function of the impression time. The steady-state creep rate, $\dot{\varepsilon}_I$, could be related to control stress (hardness, H) through a power-law relationship [16, 18].

In the indentation creep experiment, the indenter tip was subjected to a constant load during the holding period (figure 1). However, the resultant stress (hardness) was not

constant, since the indenter–sample contact area continuously increases during the indenter holding period. Thus, a single representative hardness cannot be used to accurately describe the controlled stress during the indentation creep. Instead, the instantaneous indentation hardness (H) should be used:

$$H = \frac{P}{\pi a^2}, \tag{4}$$

where P and a are the instantaneous indentation load and indenter–sample contact radius, respectively.

The deformation under an indenter is known to differ from that occurring in a uniaxial test. The mode of indentation deformation under a blunt indenter for an isotropic material resembles a cavity expansion, as originally proposed by Bishop *et al* [29]. According to this model, the material directly adjacent to the indenter will be plastically deformed, while the material far from the indenter will be elastically loaded. Between the two regions is an elastic–plastic boundary or the cavity boundary. The cavity expansion model has been extended recently to the indentation of transversely isotropic foam material by Tagarielli *et al* [33]. Overall, the cavity shape (the cavity boundary) of a transversely isotropic material is found to be similar to that of an isotropic material. Inside the boundary the material is fully densified while the material outside the band is elastic. During the steady-state creep, the cavity boundary proceeds at a constant speed. It is reasonable to postulate that the size of the cavity boundary is related to the size of the indenter–sample contact area [30–33]. Thus, the indentation strain rate ($\dot{\varepsilon}_\mathrm{I}$) can be defined as

$$\dot{\varepsilon}_\mathrm{I} = \frac{\dot{A}}{A} = \frac{\dot{a}}{a}, \tag{5}$$

where $\dot{A}$ is the instantaneous change in contact area and A the instantaneous contact area, and $\dot{a}$ is the instantaneous change in contact radius and a the instantaneous contact radius.

The indenter–sample contact radius (a) is computed via equation (2) and the derivative of the a–t curve at the steady-state region yields the change in contact radius ($\dot{a}$). The ratio of $\dot{a}/a$ is the indentation strain rate (equation (5)). Equations (4) and (5) allowed the tabulation of instantaneous indentation hardness–strain rate pairs. The hardness–strain rate pairs were then plotted on a log–log graph and the slope yielded the strain rate sensitivity, m:

$$m = \frac{\partial \ln H}{\partial \ln \dot{\varepsilon}_\mathrm{I}}. \tag{6}$$

The plots of $\ln(H)$ versus $\ln(\dot{\varepsilon}_\mathrm{I})$ for the VA-CNT arrays are shown in figure 6. It is seen that the relation between the hardness and strain rate for each CNT array is linear (the coefficient of correlation >0.99) at large displacements, corresponding to the steady-state creep. The slopes of $\ln(H)$–$\ln(\dot{\varepsilon}_\mathrm{I})$ curves yield the strain rate sensitivities. The VA-CNT array with a higher tube density is seen to have a smaller strain rate sensitivity, $m_1 = 0.013$. The time-dependent deformation is thus affected by the 'density' of the nanotube arrays. The denser the tube material, the fewer the geometric freedoms for tube movement, and thus the less creep deformation.

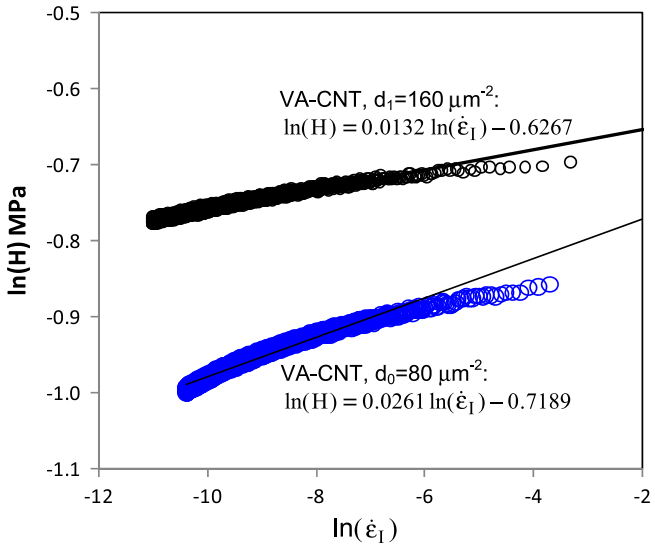

Figure 6. Indentation hardness versus strain rate curves for the VA-CNT arrays.

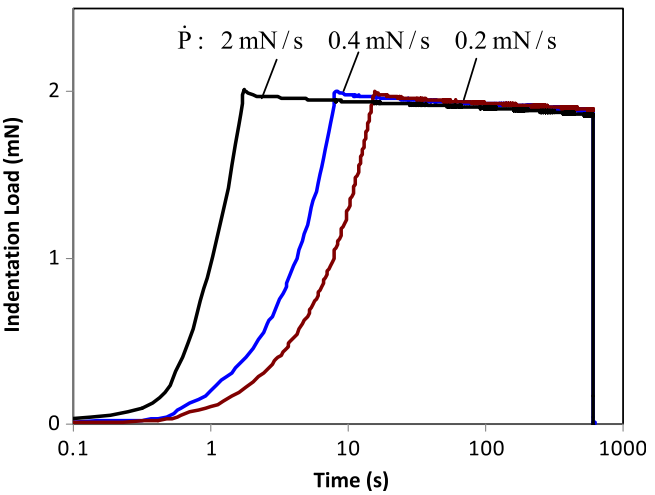

Figure 7. The load–time profiles used to examine the effect of load ramping rates in nanoindentation creep experiments.

The strain rate sensitivity seems to be independent of the ramping rates of the indenter. The trends of $\ln(H)$–$\ln(\dot{\varepsilon}_\mathrm{I})$ curves are identical for different ramping rates from 0.14 mN s^{-1} through 0.28 mN s^{-1} to 1.4 mN s^{-1} (figure 7), and the resultant strain rate sensitivities are also approximately the same (figure 8). This finding is consistent with the results reported for polymers [16] and metals [15].

The mechanism of creep is known to vary from material to material. Depending on the microstructure and operative temperatures, different creep mechanisms apply even for the same material [34, 35]. This paper is probably the first to report the viscoelastic creep phenomena occurred in VA-CNT arrays. A thorough understanding about the creep mechanism of the VA-CNTs would require further experimental investigations, along with the development of proper rheological models. To a first approximation, we attribute the viscous creep to the complex microstructure of the CNT array itself. Although the present CNTs are nominally aligned and straight, the actual shapes of the tubes are helical (figure 2(*c*)). The macro-scale

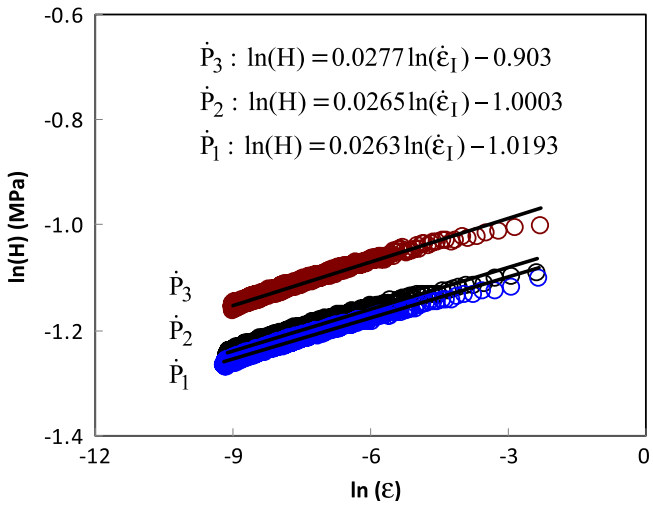

Figure 8. Indentation hardness versus strain rate curves obtained at various load ramping rates: $\dot{P}_1 = 0.14\,\mathrm{mN\,s^{-1}}$, $\dot{P}_2 = 0.28\,\mathrm{mN\,s^{-1}}$, $\dot{P}_3 = 1.4\,\mathrm{mN\,s^{-1}}$.

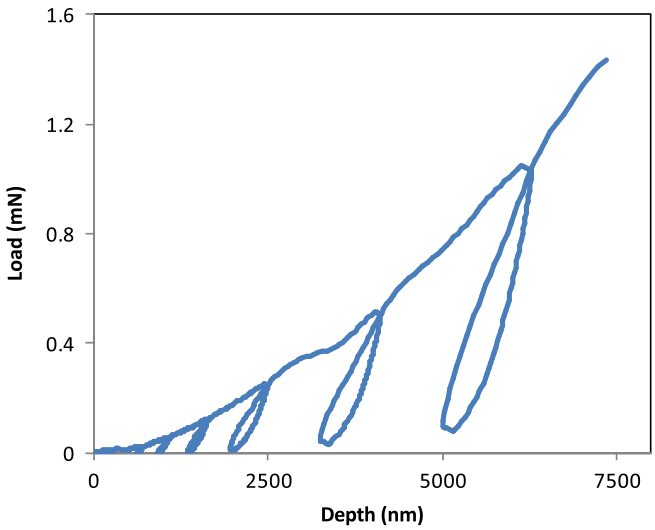

Figure 9. Cyclic indentation load–depth curve showing the presence of hysteresis in the VA-CNT array.

helical springs are known to exhibit viscoelastic behaviour due to their ability to dissipate mechanical energy [36]. It is expected that the nano-scale helical springs will inherit the same property. The creep response is further considered to be the result of contact deformation and friction between the CNTs, a mechanism that has been used to explain the relaxation in CNT arrays [8]. Under the compression of a blunt indenter, the individual tubes first bend (an elastic, time-independent deformation), and then begin to contact with neighbouring tubes. When the indenter load is held constant over time, the changes in contacts may still continue. The contact deformation (such as sliding) dissipates energy, which is evidenced by the hysteresis loops observed in the indenter loading–unloading cycle (figure 9). The hysteresis is a property of materials as a result of the local stress distribution (in this case the interfacial contact stresses between the inter-CNTs), and increases proportionally to the pre-strain.

4. Conclusions

Viscous creep in VA-CNTs has been measured from the nanoindentation experiment. In the test, the indenter is quickly ramped to a control load and then held at the peak for a period of time. Resulting creep response is seen to consist of two stages: (1) a short transient stage and (2) a steady-state stage, in which the rate of displacement is constant. The instantaneous control stress (hardness, H) and strain rate ($\dot{\varepsilon}_I$) are monitored during the experiment, and the slope of the $\ln(H)$–$\ln(\dot{\varepsilon}_I)$ curve yields the strain rate sensitivity of the nanotube material. The instantaneous modulus of the VA-CNT array was found to be 58 MPa, though the axial modulus of a single SWNT could be as high as 1 TPa. The strain rate sensitivity depends on the density of the nanotube arrays. Denser nanotube material has fewer geometric freedoms for the tube movement, and thus less creep deformation. It was demonstrated that the strain rate sensitivity of the VA-CNT array decreased by a factor of 2 simply by doubling the nanotube density.

Acknowledgments

Y C Lu thanks AFRL and NASA EPSCoR Research Infrastructure Development (RID) Program for financial support. L Dai thanks AFRL and NSF (CMMI-0609077) for financial support.

References

[1] Fan S, Chapline M G, Franklin N R, Tombler T W, Cassell A M and Dai H 1999 Self-oriented regular arrays of carbon nanotubes and their field emission properties *Science* **283** 512

[2] Kreupl F, Graham A P, Duesberg G S, Steinhögl W, Liebau M, Unger E and Hönlein W 2002 Carbon nanotubes in interconnect applications *Microelectron. Eng.* **64** 399–408

[3] Xu J and Fisher T S 2006 Enhancement of thermal interface materials with carbon nanotube arrays *Int. J. Heat Mass Transfer* **49** 1658–66

[4] McCarter C M, Richards R F, Mesarovic S Dj, Richards C D, Bahr D F, McClain D and Jiao J 2006 Mechanical compliance of photolithographically defined vertically aligned carbon nanotube turf *J. Mater. Sci.* **41** 7872–8

[5] Bajpai V, Dai L and Ohashi T 2004 Large-scale synthesis of perpendicularly aligned helical carbon nanotubes *J. Am. Chem. Soc.* **126** 5070–1

[6] Zhang Q, Liu J, Sager R, Dai L and Baur J 2009 Hierarchical composites of carbon nanotubes on carbon fiber: influence of growth condition on fiber tensile properties *Compos. Sci. Technol.* **69** 594

[7] Patton S T, Zhang Q, Qu L, Dai L, Voevodin A A and Baur J 2009 Electromechanical characterization of carbon nanotube grown on carbon fibers *J. Appl. Phys.* **106** 104313

[8] Mesarovic S Dj, McCarter C M, Bahr D F, Radhakrishnan H, Richards R F, Richards C D, McClain D and Jiao J 2007 Mechanical behavior of a carbon nanotube turf *Scr. Mater.* **56** 157–60

[9] Pathak S, Goknur Cambaz Z, Kalidindi S R, Gregory Swadener J and Gogotsi Y 2009 Viscoelasticity and high buckling stress of dense carbon nanotube brushes *Carbon* **47** 1969–76

[10] Misra A, Greer J R and Daraio C 2008 Strain rate effects in the mechanical response of polymer-anchored carbon nanotube foams *Adv. Mater.* **21** 334–8

[11] Pollock H M, Maugis D and Barquins M 1986 Characterization of sub-micrometer layers by indentation *Microindentation Techniques in Materials Science and Engineering* ed P J Blau and B R Lawn (Philadelphia, PA: ASTM) pp 47–71
[12] Mayo M J, Siegel R W, Liao Y X and Nix W D 1992 Nanoindentation of nanocrystalline ZnO *J. Mater. Res.* **7** 973–9
[13] Mayo M J, Siegel R W, Narayanasamy A and Nix W D 1990 Mechanical properties of nanophase TiO_2 as determined by nanoindentation *J. Mater. Res.* **5** 1073–82
[14] Mayo M J and Nix W D 1988 *Strength of Metals and Alloys* ed P O Kettunen *et al* (Elmsford, NY: Pergamon) pp 1415–20
[15] Poisl W H, Oliver W C and Fabes B D 1995 The relationship between indentation and uniaxial creep in amorphous selenium *J. Mater. Res.* **10** 2024–32
[16] Lu Y C, Tandon G P, Putthanarat S and Schoeppner G A 2009 Nanoindentation strain rate sensitivity of thermo-oxidized PMR-15 Polyimide *J. Mater. Sci.* **44** 2119–27
[17] Taljat B and Pharr G M 2004, Development of pile-up during spherical indentation of elastic–plastic solids *Int. J. Solids Struct.* **41** 3891–904
[18] Cheng Y T and Cheng C M 2004 Scaling, dimensional analysis, and indentation measurements *Mater. Sci. Eng.* R **44** 91
[19] Lu Y C, Jones D C, Tandon G P, Putthanarat S and Schoeppner G A 2010 High temperature nanoindentation of PMR-15 polyimide *Exp. Mech.* **50** 491–9
[20] Oliver W C and Pharr G M 1992 An improved technique for determining hardness and elastic modulus using load and displacement sensing indentation experiments *J. Mater. Res.* **7** 1564
[21] 2004 *MTS Manual: Theory & Practice of Instrumented Indentation Testing (IIT)* (Oak Ridge, TN: MTS Systems Corporation)
[22] Zbib A A, Mesarovic S Dj, Lilleodden E T, McClain D, Jiao J and Bahr D F 2008 The coordinated buckling of carbon nanotube turfs under uniform compression *Nanotechnology* **19** 175704
[23] Cao A, Dickrel P L, Sawyer W G, Ghasemi-Nejhad M N and Ajayan P M 2005 Super-compressible foamlike carbon nanotube films *Science* **310** 1307–13
[24] Wardle B L, Saito D S, García E J, Hart A J, de Villoria R G and Verploegen E A 2008 Fabrication and characterization of ultra-high volume fraction aligned carbon nanotube polymer composites *Adv. Mater.* **20** 2707
[25] Liew K M, Wong C H and Tan M J 2006 Tensile and compressive properties of carbon nanotube bundles *Acta Mater.* **54** 225–31
[26] Treacy M M J, Ebbesen T W and Gibson J M 1996 Exceptional high Young's modulus observed for individual carbon nanotubes *Nature* **381** 678
[27] Pantano C H, Boyce M C and Parks D M 2004 Mechanics of deformation of single and multiwalled carbon nanotubes *J. Mech. Phys. Solids* **52** 789–821
[28] Qi H J, Teo K B K, Lau K K S, Boyce M C, Milne W I, Robertson J and Gleason K K 2003 Determination of mechanical properties of carbon nanotubes and vertically aligned carbon nanotube forest using nanoindentation *J. Mech. Phys. Solids* **51** 2213–37
[29] Bishop R E, Hill R and Mott N F 1945 The theory of indentation and hardness tests *Proc. Phys. Soc.* **57** 147
[30] Biwa S and Storakers B 1995 An analysis of fully plastic Brinell indentation *J. Mech. Phys. Solids* **43** 1303–33
[31] Bower A F, Fleck N A, Needlman A and Ogbonna N 1993 Indentation of a power law creeping solid *Proc. R. Soc.* A **441** 97
[32] Lu Y C and Shinozaki D M 1998 Deep penetration microindentation of high density polyethylene *Mater. Sci. Eng.* A **249** 134
[33] Tagarielli V L, Deshpande V S, Fleck N A and Chen C 2005 A constitutive model for transversely isotropic foams and its application to the indentation of balsa wood *Int. J. Mech. Sci.* **47** 666–86
[34] Frost H J and Ashby M F 1982 *Deformation-Mechanism Maps* (Oxford: Pergamon)
[35] Sargent P and Ashby M F 1992 Indentation creep *Mater. Sci. Technol.* **8** 594
[36] Hanna W D, Chang D J and Steckel G L 1998 Stress relaxation of spring materials *Proc. 32nd Aerospace Mechanism Symp. (Cocoa Beach, FL, 13–15 May)* ed S W Walker and E A Boesigner